



Published in final edited form as:

BBA Adv. 2021 ; 1: . doi:10.1016/j.bbadv.2021.100020.

Fragments of *Locusta migratoria* apoLp-III provide insight into lipid binding

Blair A. Russell,

James V.C. Horn,

Paul M.M. Weers*

Department of Chemistry and Biochemistry, California State University Long Beach, 1250 Bellflower Blvd, Long Beach, CA 90840, United States

Abstract

Apolipoprotein III (apoLp-III) from *Locusta migratoria* is an exchangeable apolipoprotein with a critical role in lipid transport in insects. The protein is composed of a bundle of five amphipathic α -helices which undergo a large conformational change upon lipid binding. To better understand the apoLp-III lipid binding interaction, the protein was cleaved by cyanogen bromide upon introduction of a S92M mutation, generating an N-terminal fragment corresponding to the first three helices (NT_{H1-3}) and a C-terminal fragment of the last two helices (CT_{H4-5}). MALDI-TOF analysis of the HPLC purified fragments provided masses of 9863.8 Da for NT_{H1-3} and 7497.0 Da for CT_{H4-5} demonstrating that the intended fragments were obtained. Circular dichroism spectra revealed a decrease in helical content from 82% for the intact protein to 57% for NT_{H1-3} and 41% for CT_{H4-5}. The fragments adopted considerably higher α -helical structure in the presence of trifluoroethanol or phospholipids. Equimolar mixing of the two fragments did not result in changes in helical content or tryptophan fluorescence, indicating recombination into the native protein fold did not occur. The rate of protein induced dimyristoylphosphatidylcholine vesicle solubilization increased 15-fold for NT_{H1-3} and 100-fold for CT_{H4-5} compared to the intact protein. Despite the high activity in phospholipid vesicle interaction, CT_{H4-5} did not protect phospholipase-treated low-density lipoprotein from aggregation. In contrast, NT_{H1-3} provided protection to lipoprotein aggregation similar to the intact protein, indicating that specific amino acid residues in this part of apoLp-III are essential for lipoprotein binding interaction.

Keywords

Apolipoprotein; Apolipoprotein; Phospholipid; Diacylglycerol

Introduction

Apolipoprotein III (apoLp-III) is a small 18 kDa exchangeable apolipoprotein found abundantly in the hemolymph of a number of insect species that rely heavily on lipids to

fuel flight activity [1]. The role of apoLp-III in mobilizing fat body triacylglycerol reserves has been well established and involves a dynamic lipophorin shuttle mechanism that depends on apoLp-III association with diacylglycerol-enriched lipophorins [2]. Initial biophysical studies of apoLp-III and elucidation of the X-ray structure provided important insight into how apoLp-III interacts with lipid surfaces through large conformational changes [3–7]. NMR solution structures of apoLp-III of two different species became available [8,9], making the protein an attractive model exchangeable apolipoprotein to gain insight into the structure-function relationship [1]. ApoLp-III in the lipid-free state is comprised of a helix bundle with helices arranged in an up-and-down topology [6]. However, instead of the common 4-helix protein fold, apoLp-III is a bundle of five antiparallel α -helices. It is thought that the 5-helix bundle conformation results in a lower protein stability, facilitating helix repositioning during lipid binding [8,10]. The α -helices are amphipathic, with hydrophobic side chains orienting towards the protein interior. A large conformational change exposes the hydrophobic faces of the α -helices, providing the protein with strong lipid binding properties [3,7].

The development of bacterial expression systems facilitated the use of site-directed mutagenesis to introduce point-mutations in apoLp-III [11–14]. This structure-guided mutagenesis approach has provided additional insights in apoLp-III lipid binding, which revealed some striking similarities with vertebrate apolipoproteins [15]. While the three-dimensional structure of apoLp-III from *Locusta migratoria* (apoLp-III_{LM}) has been known for almost thirty years, the lipid-bound conformation has remained elusive. Several models based on the high-resolution structure and biophysical analysis of lipid-free apoLp-III have been developed that describe the opening of the helix bundle [6,9, 16]. The models differ in how the individual helices move away from each other to open the protein interior allowing the hydrophobic amino acids to make contact with the lipid surface. Other insights into the apoLp-III lipid binding interactions were provided by studies using truncation variants of apoLp-III. These studies showed that helix removal resulted into a much reduced protein stability, but strongly enhanced ability to solubilize phospholipid vesicles, a hallmark feature of exchangeable apolipoproteins [17–19]. An earlier study showed that when apoLp-III_{LM} was cleaved in the middle of helix-3, two fragments of similar size were produced with lower lipid binding properties [20]. Since helix-3 was compromised, this may have affected the lipid binding properties of the peptides. To better understand which part of apoLp-III harbors the helices critical for lipid binding, apoLp-III_{LM} was cleaved into two fragments while preserving the helix boundaries. Ser-92, residing in the loop connecting helix- 3 and -4, was substituted by a methionine residue. This apoLp-III-S92M variant was then cleaved with cyanogen bromide (CNBr) to generate an N-terminal (NT) fragment with three potential helical segments, and a C-terminal (CT) fragment with two helices. While the helical structure was decreased, phospholipid solubilization was remarkably improved for both fragments, however, the smaller CT fragment lacked lipoprotein binding capabilities.

2. Materials and methods

2.1. Site-directed mutagenesis and recombinant protein expression and purification

The coding region of apoLp-III was inserted into the pET22b(+) vector as described previously [12]. To introduce the S92M mutation, the QuickChange-II site-directed mutagenesis kit (Agilent) was used with the following two primers (Eurofins): 5'CGACGCCACGATGCTCAACCTGCAGG-3' (forward) and 5'-CCTGCAGGTTGAGCATCGTGGCGGCGTCG-3' (reversed). The mutation was verified by DNA sequencing. Recombinant wild-type apoLp-III and apoLp-III-S92M were produced in a well-established *Escherichia coli* recombinant expression system, using the pET22b+ vector [12]. The protein isolated from insects is glycosylated at two Asn residues, but the recombinant protein contains no carbohydrates [21]. Cultures were grown in minimal medium M9 minimal media supplemented with 13.3 mM glucose, 0.1 mM CaCl₂, 2 mM MgSO₄ and protein overexpression was induced when the optical density at 600 nm reached 0.6 by 0.5 mM isopropylthiogalactopyranoside, and apoLp-III accumulated in the culture medium. Proteins were concentrated using a 10 kDa ultrafiltration membrane (Millipore, Billerica, MA) to an approximate volume of 10 mL. ApoLp-III was purified in a two-step process using Sephadex G75 gel filtration chromatography and reversed-phase HPLC (Ultimate 3000, Thermo Scientific, Waltham, MA). Each protein expression yielded approximately 20 mg of pure protein per L of *E. coli* culture. The purity of apoLp-III preparations was verified by sodium dodecyl sulfate polyacrylamide gel electrophoresis (SDS-PAGE), using precast 10% NuPAGE Bis-Tris precast gels (Invitrogen, Carlsbad, CA) using 2-(N-morpholino) ethanesulfonic acid buffer, applying 200 Volts for 30 min during electrophoresis. Gels were stained for 30 min with naphthol blue black (45% methanol; 45% H₂O, 10% acetic acid, 0.5% naphthol blue black). Purified proteins were freeze-dried (Free Zone, Labconco, Kansas City, MO) and stored at -20 °C until use. Prior to analysis, dried proteins were dissolved in the appropriate buffer, and protein concentrations were subsequently measured with the bicinchoninic acid assay (Thermo Scientific, Waltham, MA) using bovine serum albumin as a standard. Absorbance measurements were carried out with a Varioskan Lux Plate reader (Thermo Scientific, Waltham, MA) at 562 nm. The final protein concentration was calculated using the standard curve generated with BSA.

2.2. Cyanogen bromide cleavage

To cleave apoLp-III into two fragments, 35 mg of lyophilized apoLp-III-S92M was dissolved in 0.5 mL of 70% formic acid containing 21 mg CNBr (Aldrich Chemistry, St. Louis, MO), which corresponded to a 1:100 molar ration of methionine to CNBr. The CNBr reaction was carried out at room temperature for 24 h, followed by inactivation by addition of five volumes of H₂O, and the solution was freeze-dried. Protein was then dissolved in 200 mM Tris-base, pH 11.3 to neutralize formic acid. This was followed by dialysis in 20 mM sodium phosphate, pH 7.2 in Spectra/Por cellulose dialysis tubing with a 3.5 kDa cut off (Spectrum Laboratories, Rancho Dominguez, CA). The protein fragments were purified using reversed-phase HPLC, using a gradient of H₂O and acetonitrile in 0.05% trifluoroacetic acid at a flow rate of 0.7 mL/min. The eluate was monitored by measuring the absorbance at 225 nm. When the protein eluted, one-min fractions were collected, which were analyzed by SDS-PAGE as described above. Fractions corresponding to NT or CT

fragments were pooled, freeze-dried, and stored at $-20\text{ }^{\circ}\text{C}$ for later use. The molecular mass of the fragments was determined in an AB SCIEX 4800 MALDI mass spectrometer using sinapinic acid as the matrix at the IIRMES facility at CSU Long Beach.

2.3. Far UV circular dichroism

Secondary structure characterization of apoLp-III samples was performed by far UV circular dichroism (CD) using a Jasco 810 polarimeter (Jasco Instruments, Easton, MD) as described previously [17]. Protein samples were analyzed at a concentration of 0.2 mg/mL in 20 mM sodium phosphate (pH 7.2), in the absence or presence 50:50 (v/v) 2,2, 2-trifluoroethanol (TFE). To measure recombination of the two fragments, NT and CT fragments were mixed in equimolar ratio (0.2 mg/mL total protein concentration) and incubated at room temperature for 2 h prior to CD analysis. Further, far UV spectra were obtained of proteins that adopted the lipid bound state by incubation with DMPC at $24.1\text{ }^{\circ}\text{C}$ as described in Section 2.5. Molar ellipticity was calculated using the following equation in which MRW is the mean residual weight, θ_{λ} is the observed ellipticity in millidegrees, l is the path length (cm) and c is the concentration of protein (g/mL):

$$[\theta]_{222} = \frac{\text{MRW} \cdot \theta_{\lambda}}{l \cdot c}$$

Percent α -helical content was calculated using the following equation based on the molar ellipticity at 222 nm:

$$\% \alpha \text{ helix} = 100 \cdot \frac{-\theta_{222} + 3,000}{(39,000)}$$

Helical content was further calculated using DICHROWEB algorithms using the following inputs: Jasco 1.50 file format, ellipticity in millidegrees, initial wavelength 260 nm, final wavelength 185 nm, wavelength step 0.2; lowest data point at 185 nm. Analysis programs were CDSSTR, Contin, and Selcon3 using SP175 reference set [22].

2.4. Fluorescence analysis

Tryptophan fluorescence of apoLp-III was measured in a LS 55 fluorescence spectrometer (PerkinElmer, Waltham, MA). Protein samples of 30 $\mu\text{g/mL}$ in phosphate buffered saline (PBS; 37 mM NaCl, 2.7 mM KCl, 10 mM Na_2HPO_4 , 1.8 mM KH_2PO_4 , pH 7.4) were transferred to a quartz cuvette (Starna Cells, Atascadero, CA), and samples were excited at 280 nm with a slit width of 3 nm. Emission was monitored from 290 to 450 nm at a scan rate of 50 nm/min using five accumulation cycles. The exposed hydrophobic surface was measured with 8-anilino-naphthalene-1-sulfonic acid (ANS)(Sigma-Aldrich, St. Louis, MO). Protein samples (5 μM final concentration) were mixed with ANS (230 μM final concentration) in 1 mL total volume in a quartz cuvette (Starna Cells, Atascadero, CA). Samples were excited at 395 nm, with a slit width of 6 nm, and emission was monitored from 400 to 650 nm, using 3 accumulation cycles at a scan rate of 50 nm/min.

2.5. Vesicle solubilization

Anhydrous 1,2-dimyristoyl-sn-glycero-3-phosphocholine (DMPC) was obtained from Avanti Polar Lipids, Alabaster, AL. DMPC was dissolved in 1 mL of a chloroform-methanol mixture (3:1 by volume) and solvent was evaporated with N₂ gas. The resulting lipid film was dried for 16 h in a freeze-dryer. The lipid film was resuspended in PBS and incubated in a 42 °C water bath for 1 min, and vortexed rigorously for 1 min to obtain multilamellar vesicles. The vesicles were extruded 15 times through 200 nm membranes (Whatman nucleopore track-etch) assembled in a mini-extruder (Avanti Polar Lipids, Alabaster, AL) at 24 °C to form large unilamellar vesicles (LUV). To measure protein-induced phospholipid vesicle solubilization, 250 µg LUVs were equilibrated at 23.9 °C in a Genesys 150 UV-visible spectrophotometer (Thermo Scientific, Waltham, MA). Upon equilibration, 125 µg protein was added (1 mL final volume), and the absorbance at 325 nm was measured for 5 min. Rate constants were calculated assuming first order kinetics.

2.6. Lipoprotein binding

Fifty µg protein of human low-density lipoprotein (LDL, Sigma-Aldrich, St. Louis, MO) was mixed with 25, 50, or 100 µg of intact apoLp-III or one of the apoLp-III fragments in 50 mM Tris-HCl, 150 mM NaCl, 2 mM CaCl₂, pH 7.4. The reaction was started by adding 160 mU phospholipase-C (PL-C) from *Bacillus cereus* (Sigma-Aldrich, St. Louis, MO) and the mixture was incubated at 37 °C for 120 min. Reactions were carried out in a 96-microwell plate, with a total volume of 200 µL. LDL aggregation was monitored every 5 min by measuring the absorbance at 340 nm in a Varioskan LUX multimode microplate reader (ThermoScientific, Waltham, MA).

2.7. Protein crosslinking

Anhydrous dimethyl suberimidate (DMS, Thermo Scientific, Waltham, MA) was resuspended in 500 µL of triethanolamine to obtain a 11 mg/mL stock solution. Samples of 30 µg protein in 20 mM sodium phosphate buffer (pH 7.2) were mixed with 2.5 µL of the DMS stock solution in a total volume of 40 µL. Samples were allowed to react with DMS for 2 h at 25 °C before analysis by SDS-PAGE.

2.8. Statistical analysis and molecular graphics

Experimental analysis of Far UV circular dichroism, vesicle solubilization, tryptophan fluorescence, and vesicle solubilization was carried out in triplicate unless mentioned otherwise. To determine statistical difference, one-way ANOVA with $p > 0.05$ was employed. Molecular graphics was performed with UCSF Chimera, developed by the Resource for Biocomputing, Visualization, and Informatics at the University of California, San Francisco, with support from NIH P41-GM103311 [23]. The graphical abstract was created with [BioRender.com](https://www.biorender.com).

3. Results

3.1. Generation of ApoLp-III NT and apoLp-III CT fragments

To cleave apoLp-III into two fragments, S92 was replaced by methionine by site-directed mutagenesis. The wild-type protein does not contain methionine, and the mutation allows for CNBr cleavage in the loop segment connecting helix 3 and 4. This results in a three helix NT fragment (NT_{H1-3}) and a two helix CT fragment (CT_{H4-5}), as depicted in Fig.1. The 92 residues of the NT fragment include helix-1 (residues 8–33), helix-2 (residues 38–64) and helix-3 (residues 68–91), while helix 4 (residues 97–123) and helix-5 (131–159) reside in the 70 residue CT fragment. Note that the b-isoform of apoLp-III_{LM} was used which lacks the first two amino acid residues and is 162 residues long, and amino acid numbering starts with Asp-1 [24]. The CT fragment harbors tryptophan residues at position 113 and 128, and a small helical segment spanning residues 126 to 130. After treatment with CNBr, the digest was analyzed by SDS-PAGE revealing a decrease of the apoLp-III band intensity, while two new small protein bands appeared with molecular masses of approximately 10 and 6 kDa (Fig. 2). The two fragments were purified by reversed-phase HPLC, and mass spectrometry provided a mass of 9863.8 Da for the NT_{H1-3} fragment, and 7497.0 Da for the CT_{H4-5} fragment. While the experimental mass was close to the expected mass of the CT fragment based on the amino acid sequence (7499.2 Da), the mass of the NT fragment was 20 Da larger than predicted. The expected mass was corrected for elimination of the S-CH₃ group as a result of the CNBr cleavage reaction, and the additional 20 Da could have been caused by a sodium adduct.

3.2. Structural characterization with circular dichroism

To determine if the fragments retained their helical structure, far UV CD scans were obtained. The CD plots for intact apoLp-III showed a highly α -helical character, with two prominent troughs at 208 and 222 nm (Fig 3A). Calculations with the DichroWeb CDSSTR algorithm revealed an 82% α -helical content, which is similar compared to the X-ray structure (78%, Protein Data Bank ID 1AEP) or the NMR solution structure (82 %, 1LS4). Table 1 lists the helical contents based on the CDSSTR, CONTIN, and SELCON3 methods, as well as values determined based on the molar ellipticity at 222 nm. The CNBr digestion decreased the helical content significantly. The ellipticity plot of the NT_{H1-3} fragment showed lower amplitudes of the peak at 191 nm and troughs at 208 and 222 nm. Helical content calculations provided values between 49 and 58 %, depending on the method used. The far UV CD spectrum of apoLp-III-CT_{H4-5} showed a single trough at 202 nm, indicating a further shift towards random conformation. DichroWeb calculations provided α -helical contents of 41–44 %, while 20% was predicted using the molar ellipticity at 222 nm.

To assess if the two fragments could recombine and reform the native protein structure, apoLp-III-NT_{H1-3} and -CT_{H4-5} were mixed using a 1 to 1 molar ratio. However, the far UV CD profile of the combined fragments did not match that of intact apoLp-III and was more consistent with a mixture of isolated NT_{H1-3} and CT_{H4-5} fragments. Further, the α -helical content of the NT_{H1-3} and CT_{H4-5} mixture was estimated at 48%, similar to the average

of the two individual fragments. This result suggests that mixing the NT_{H1-3} and CT_{H4-5} fragments did not result in a recombination of the 5-helix bundle.

To test whether the fragments retained their ability to adopt a helical conformation, spectra were obtained in 50% TFE, a known inducer of secondary structure [25]. Further, the effect of DMPC on the secondary structure was evaluated, this after incubating apoLp-III with DMPC at the phospholipid transition temperature to allow formation of discoidal complexes. In case of NT_{H1-3}, both TFE and DMPC increased the helical content to values similar to that of the intact protein (Fig. 3B). When the CT_{H4-5} fragment was exposed to TFE or DMPC, a shift in the ellipticity profile towards a more structured state was observed, indicated by the troughs at 208 and 222 nm (Fig. 3C). Helical content calculations showed an increase from 41% to 57% (TFE) or 58% (DMPC), an increase of ~16%.

3.3. Tryptophan and ANS fluorescence emission spectra

ApoLp-III contains tryptophan residues at position 113 and 128 which both reside in the CT_{H4-5} fragment. Upon excitation, the intact protein showed an emission fluorescent maximum (λ_{\max}) at 336.0 nm (Fig. 4). This is in agreement with a previous study where single tryptophan mutant analysis revealed that Trp-113 is buried in the helix bundle while Trp-128 resides in a loop resulting in partial exposure to solvent, yielding a combined emission spectrum centered around 335 nm [26]. The emission spectrum of the CT_{H4-5} fragment showed a large red shift with a λ_{\max} of 362.0 nm. Since the emission spectrum of L-tryptophan yielded a λ_{\max} of 365.0 nm (not shown), the tryptophan residues in the CT_{H4-5} fragment were fully exposed to buffer. ApoLp-III-NT_{H1-3} lacks tryptophan, and thus the fluorescence emission intensity was negligible. Mixing the NT_{H1-3} and CT_{H4-5} fragments in an equimolar ratio did not change the fluorescence emission spectrum. This suggests that the NT_{H1-3} and CT_{H4-5} fragments did not recombine to form a closed helical bundle at the conditions employed, in agreement with the far UV CD data.

ANS fluorescence was used to probe for hydrophobic pockets on the protein surface, which could promote lipid binding interactions. ANS binding to proteins is evident by a blue-shift of λ_{\max} and increase in fluorescence intensity. The λ_{\max} of ANS in the absence of protein was 518.0 nm with an emission intensity of 147.4 ± 1.7 (Fig. 5). The ANS fluorescence intensity increased in the presence of intact apoLp-III to 227.4 ± 18.6 with a λ_{\max} of 498.0 nm. The emission profiles for the two fragments were similar to ANS in the absence of protein, with a λ_{\max} of 518.5 nm and emission intensity of 166.5 ± 18.3 for the NT_{H1-3} fragment, and a λ_{\max} of 519.5 nm and emission intensity of 154.8 ± 9.7 for the CT_{H4-5} fragment. Since ANS spectra of the NT_{H1-3} and CT_{H4-5} fragments lacked a blue-shift and increase in fluorescence intensity, this indicates a lack of ANS binding sites, and therefore may not contain exposed hydrophobic surfaces.

3.4. Protein crosslinking

The Far-UV CD profiles indicated that the NT_{H1-3} fragment retained more helical character compared to CT_{H4-5}. This raised the question of how this structure was stabilized, and the possibility of self-association was assessed. To measure this, proteins were incubated with DMS crosslinker, which forms covalent bonds between lysine side chains that are in close

proximity. ApoLp-III_{LM} harbors eight lysine residues, four in each fragment. Intermolecular crosslinking was analyzed by SDS-PAGE (Fig. 6). DMS treatment of intact apoLp-III did not result in formation of high molecular mass complexes, in agreement with the well-established monomeric character of the protein. In contrast, apoLp-III-NT_{H1-3} showed extensive crosslinking. In addition to the monomer at 18 kDa, dimers, trimers, tetramers, and higher molecular mass complexes appeared on the gel. DMS crosslinked CT_{H4-5} fragments were also visible, but to a lesser extent compared to apoLp-III-NT_{H1-3}. This suggests that the helical structure of the NT fragment was stabilized by self-association.

3.5. DMPC vesicle solubilization

To determine the lipid binding activity of the two fragments, the rate of protein-induced solubilization of DMPC vesicles was measured at the phospholipid transition temperature of 24.1 °C. The LUVs used in the present study had a diameter of 200 nm, resulting in extensive light scatter at 325 nm. The transformation of LUVs into small discoidal particles, ~15 nm diameter for apoLp-III/DMPC complexes [5], was monitored by the decrease in light scatter intensity. As shown in Fig. 7, solubilization of LUVs by intact apoLp-III was relatively slow, 250 s was required for the light scatter intensity to decrease by ~50%. In contrast, the rate of vesicle solubilization by NT_{H1-3} was much improved, and only 10 s were needed to achieve 50% solubilization. Remarkably, it took the CT_{H4-5} fragment only a few seconds solubilize 50% of the vesicles. Rate constants calculations assuming exponential decay kinetics yielded values of $2.77 \pm 0.33 \cdot 10^{-3} \text{ s}^{-1}$ for intact apoLp-III, 38.96 ± 1.32 for apoLp-III-NT_{H1-3} and 270.03 ± 1.13 for apoLp-III-CT_{H4-5} (n = 3, ± SD). Thus, vesicle solubilization rates were 14 times faster for NT_{H1-3} and ~100 times faster for CT_{H4-5} fragments compared to intact apoLp-III.

3.6. Lipoprotein binding

The primary function of apoLp-III is to bind to diacylglycerol-rich lipoprotein. To mimic this process *in vitro*, human LDL was modified with PL-C, resulting in conversion of phosphatidylcholine, that resides on the lipoprotein surface and is accessible to the enzyme, into diacylglycerol (DG). This causes LDL to aggregate leading to sample turbidity, which can be monitored by measuring the absorbance at 340 nm in a spectrophotometer [27]. ApoLp-III does not bind to untreated LDL, but when LDL is incubated in the presence of PL-C, the appearance of DG provides binding sites for apoLp-III. As a result of apoLp-III binding to LDL, the onset of aggregating is prevented or delayed. As shown in Fig. 8A, PL-C addition to LDL resulted in a rapid increase in sample turbidity, while inclusion of 25 µg intact apoLp-III_{LM} into the reaction mixture kept the absorbance low until ~40 min, after which the absorbance slowly increased. Similar results were obtained for apoLp-III-NT_{H1-3}, showing that this fragment is able to bind to lipolyzed LDL, providing protection against aggregation. In contrast, apoLp-III-CT_{H4-5} did not prevent the rapid increase in sample turbidity, and LDL started to aggregate at the 15 min timepoint, reaching values similar to LDL and PL-C in the absence of intact apoLp-III. Increasing the amount of apoLp-III-CT_{H4-5} from 25 to 100 µg had no measurable effect on LDL aggregation (Fig. 8B), showing that this fragment is not effective in preventing the onset of PL-C induced LDL aggregation.

4. Discussion

In the present study the 5-helix bundle protein of apoLp-III_{LM} was cleaved into two fragments after introduction of a methionine residue at position 92. CNBr cleavage produced an NT fragment with amino acids corresponding to the first three helices and a CT fragment with the two remaining helices. Both fragments displayed a noticeable decrease in α -helical content, with the NT_{H1-3} fragment retaining more helical structure compared to the CT_{H4-5} fragment. Since the fragments showed a substantial increase in the degree of DMS crosslinking, the remaining helical structure may have been stabilized by self-association. While the two fragments lack exposed hydrophobic surfaces, they have potential to form a large hydrophobic surface upon adopting α -helical structure, which may direct reassembly into the native protein fold. However, when NT_{H1-3} and CT_{H4-5} fragments were mixed, helical content remained unchanged and CT tryptophan residues remained fully exposed, suggesting that the fragments did not recombine. Both fragments were considerably more potent in solubilizing DMPC vesicles, the rate of solubilization increased 14 times for the NT_{H1-3} and ~100 times for the CT_{H4-5} fragment compared to the intact protein. Helix 2 and 5 of apoLp-III_{LM} are considered class A, which have distinct polar and nonpolar faces, with lysine and arginine residues positioned at the hydrophobic/hydrophilic interface and aspartate and glutamate positioned at the center of the polar face [20]. It has been proposed that this arrangement provides class A amphipathic α -helices with high lipid binding potential [28]. Since both NT_{H1-3} and CT_{H4-5} fragments each contain one class A helix, this cannot explain the large difference in phospholipid vesicle solubilization rates. Previous studies have shown that apoLp-III-induced DMPC solubilization rates increase when lowering the pH, point mutations were introduced that changed the stability of the protein, or when one or more helices were removed [10, 17,19,29,30]. These studies provided evidence for an inverse correlation between helix bundle stability and vesicle solubilization rates. Thus, the relatively low stability of apoLp-III promotes helix bundle opening to facilitate lipid binding, in which helix-helix interactions are replaced by helix-lipid interactions [8]. This correlation has also been observed for human apoE, a two-domain apolipoprotein with a 4-helix bundle NT domain [31,32]. The unstructured character of both apoLp-III fragments likely promoted lipid binding when the α -helical conformation was adopted, similar as observed for human apolipoprotein A-I (apoA-I), a 243-residue plasma protein comprised of two domains [33]. The NT contains the central α -helices that form a stable helix-bundle, resembling the helix bundle of apoLp-III [34]. The CT domain of apoA-I is relatively unstructured and is made of the last ~65 residues [35]. These CT residues become α -helical when the protein switches to the lipid bound conformation [36]. Further, apoA-I lacking the CT residues is ineffective in lipid binding, and therefore these residues are thought to initiate lipid binding through formation of α -helical structure, which is thermodynamically favorable, driving the apolipoprotein-induced conversion of vesicles into discoidal particles [37].

The ability to protect PL-C treated LDL was distinctly different for the two fragments. While the NT_{H1-3} fragment provided robust protection, the CT_{H4-5} did not afford protection against PL-C induced LDL aggregation. Thus, while the CT fragment was most potent in solubilizing DMPC vesicles, it had lost its ability to protect the DG-enriched lipoproteins

from aggregating. This may be because a stable binding interaction with the lipoprotein surface could not be established, and packing defects caused by the appearance of DG could not be neutralized, and LDL continued to aggregate rapidly. Since ANS was unable to bind to either fragment, differences in exposed hydrophobic surfaces cannot explain this observation. Therefore, the data suggest the presence of specific residues in helix 1, 2 or 3 that are required for association with the modified lipoprotein surface. In contrast, the presence of amphipathic α -helices merely acting as detergent may be sufficient for DMPC vesicle solubilization and a specific sequence or motif may not be necessary. However, the rate of vesicle solubilization depends on the character of the amphipathic helices, such as hydrophobic moment and distribution of charged amino acid residues. Interestingly, a 7-residue mini-helix positioned between helix 3 and 4 in apoLp-III from *Manduca sexta* (apoLp-III_{MS}) was identified as a potential recognition site for lipid packing defects on the lipoprotein surface [38]. A shorter helix is present in apoLp-III_{LM}, positioned between helix 4 and 5 (₁₂₇AWAP₁₃₀) [9], however, these residues reside in the CT_{H4-5} fragment. On the other hand, a leucine cluster at one end of the helix bundle (L30, L32 and L93) may recognize binding sites on the lipolyzed LDL surface [39]. Further, the presence of a specific lipoprotein binding site in NT_{H1-3} may explain the lack of lipoprotein binding when apoLp-III was cleaved into two halves at Arg-80 which resides in the middle of helix 3, and points out that this helix may be critical for lipoprotein binding interaction [20].

Truncation variant studies provided additional insight into the lipoprotein binding interaction. When helix-1 or -5 was deleted from apoLp-III_{LM}, the resulting protein showed reduced helical content, lower protein stability, increased dimerization, and a 5-fold increase in DMPC vesicle solubilization rate [17]. Both truncation variants provided protection against PL-C induced LDL aggregation, with the variant lacking helix-5 offering better protection compared the variant lacking helix-1. Since both truncation variants contained the leucine cluster and the mini-helix, no additional insight into their role in lipoprotein binding was obtained. In another study two helical segments were removed from *Galleria mellonella* apoLp-III (apoLp-III_{GM}), generating variants comprising helix 1 to 3, helix 2 to 4, and helix 3 to 5 [18,19]. *G. mellonella* and *M. sexta* are sphinx moths, and apoLp-III from these two species have a nearly identical amino acid sequence and structure. These proteins also share a similar three-dimensional protein architecture with apoLp-III_{LM} despite a lack of amino acid sequence similarity [8,40]. Further, apoLp-III_{GM} has been studied extensively for its role in innate immunity [41]. The apoLp-III_{GM} truncation variant with amino acid residues corresponding to helix 1–3 behaved remarkably similar to apoLp-III_{LM}-NT_{H1-3}. The CD spectra of apoLp-III_{GM}-NT_{H1-3} indicated a decrease in α -helical content, which was restored by TFE or DMPC. Sedimentation equilibrium analysis revealed an equilibrium between a monomer and dimer, and DMPC vesicle solubilization was enhanced 5-fold. Importantly, this truncation variant and the variant comprised of helix 2–4 provided protection against PL-C induced LDL aggregation, albeit not as efficient as the intact protein. In contrast, the fragment lacking helix-1 and -2 did not protect LDL from aggregation, despite the presence of the 7-residue minihelix. Further, a peptide corresponding to helix 5 of apoLp-III_{MS} did not protect against PL-C induced lipoprotein aggregation either [42]. Thus, these results provide further evidence that residues of the first three helices play an important role in lipoprotein binding.

Association of apoLp-III to lipid is a complex process, involving helix repositioning to expose the hydrophobic protein interior to the new lipid surface, with diacylglycerol playing an important role [43,44]. Models for this lipid-induced conformational change have been proposed in which two α -helices move away from the three other α -helices, or by movement of helix-1 and -5 [6,8,9,14]. The protein forms an elongated α -helix in a discoidal DMPC particle, circumscribing the periphery of the disc [7,45,46]. Such a belt-like conformation with two elongated α -helices laying side by side on the discoidal edge was confirmed for apoA-I in a recent NMR study providing high-resolution structural detail [47]. Unfortunately, details of the association of exchangeable apolipoproteins with lipoprotein surfaces are still limited. To better understand how apoLp-III interacts with lipid vesicles and lipoproteins, future experimental studies with separate helical segments could provide new insight into the molecular details of the apoLp-III lipid binding interaction. These studies may clarify why apoLp-CT_{H4-5} outperformed apoLp-NT_{H1-3} in vesicle solubilization but failed to provide protection against lipoprotein aggregation when DG appeared on the lipoprotein surface.

Acknowledgments

The authors thank Andres Cueller, Nery Phillip Rafael, and Anthony Tabet for their valuable contributions during the early stages of the project, and Wendy Beck for engineering apoLp-III-S92M. Research reported in this publication was supported by the National Institute of General Medical Sciences of the National Institutes of Health under Award Number SC3GM089564.

Abbreviations:

ANS	8-anilino-naphthalene-1-sulfonic acid
ApoLp-III	apolipoprotein III
NT	N-terminal
CD	circular dichroism
CNBr	cyanogen bromide
CT	C-terminal
DMS	dimethyl sulfoxide
DMPC	1,2-dimyristoyl-sn-glycero-3-phosphocholine
LUV	large unilamellar vesicle
LDL	low-density lipoprotein
PAGE	polyacrylamide gel electrophoresis
PBS	phosphate buffered saline
PL-C	phospholipase-C
SDS	sodium dodecyl sulfate

TFE 2,2,2-trifluoroethanol

References

- [1]. Weers PM, Ryan RO, Apolipoprotein III: role model apolipoprotein, *Insect Biochem. Mol. Biol* 36 (2006) 231–240. [PubMed: 16551537]
- [2]. van der Horst DJ, van Hoof D, van Marrewijk WJA, Rodenburg KW, Alternative lipid mobilization: the insect shuttle system, *Mol. Cell. Biochem* 239 (2002) 113–119. [PubMed: 12479576]
- [3]. Kawooya JK, Meredith SC, Wells MA, Kézdy FJ, Law JH, Physical and surface properties of insect apolipoprotein III, *J. Biol. Chem* 261 (1986) 13588–13591. [PubMed: 3759983]
- [4]. Ryan RO, Oikawa K, Kay CM, Conformational, thermodynamic, and stability properties of *Manduca sexta* apolipoprotein III, *J. Biol. Chem* 268 (1993) 1525–1530. [PubMed: 8420928]
- [5]. Weers PM, Kay CM, Oikawa K, Wientzek M, Van der Horst DJ, Ryan RO, Factors affecting the stability and conformation of *Locusta migratoria* apolipoprotein III, *Biochemistry* 33 (1994) 3617–3624. [PubMed: 8142360]
- [6]. Breiter DR, Kanost MR, Benning MM, Wesenberg G, Law JH, Wells MA, Rayment I, Holden HM, Molecular structure of an apolipoprotein determined at 2.5-Å resolution, *Biochemistry* 30 (1991) 603–608. [PubMed: 1988048]
- [7]. Wientzek M, Kay CM, Oikawa K, Ryan RO, Binding of insect apolipoprotein III to dimyristoylphosphatidylcholine vesicles. Evidence for a conformational change, *J. Biol. Chem* 269 (1994) 4605–4612. [PubMed: 8308032]
- [8]. Wang J, Sykes BD, Ryan RO, Structural basis for the conformational adaptability of apolipoprotein III, a helix-bundle exchangeable apolipoprotein, *Proc. Natl. Acad. Sci. U. S. A* 99 (2002) 1188–1193. [PubMed: 11818551]
- [9]. Fan D, Zheng Y, Yang D, Wang J, NMR solution structure and dynamics of an exchangeable apolipoprotein, *Locusta migratoria* apolipoprotein III, *J. Biol. Chem* 278 (2003) 21212–21220. [PubMed: 12621043]
- [10]. Weers PM, Abdullahi WE, Cabrera JM, Hsu TC, Role of buried polar residues in helix bundle stability and lipid binding of apolipoprotein III: destabilization by threonine 31, *Biochemistry* 44 (2005) 8810–8816. [PubMed: 15952787]
- [11]. Ryan RO, Schieve D, Wientzek M, Narayanaswami V, Oikawa K, Kay CM, Agellon LB, Bacterial expression and site-directed mutagenesis of a functional recombinant apolipoprotein, *J. Lipid Res* 36 (1995) 1066–1072. [PubMed: 7658154]
- [12]. Weers PM, Wang J, Van der Horst DJ, Kay CM, Sykes BD, Ryan RO, Recombinant locust apolipoprotein III: characterization and NMR spectroscopy, *Biochim. Biophys. Acta* 1393 (1998) 99–107. [PubMed: 9714761]
- [13]. Soulages JL, Pennington J, Bendavid O, Wells MA, Role of glycosylation in the lipid-binding activity of the exchangeable apolipoprotein, apolipoprotein-III, *Biochem. Biophys. Res. Commun* 243 (1998) 372–376. [PubMed: 9480816]
- [14]. Soulages JL, Arrese EL, Chetty PS, Rodriguez V, Essential role of the conformational flexibility of helices 1 and 5 on the lipid binding activity of apolipoprotein-III, *J. Biol. Chem* 276 (2001) 34162–34166. [PubMed: 11443139]
- [15]. Narayanaswami V, Kiss RS, Weers PM, The helix bundle: a reversible lipid binding motif, *Comp. Biochem. Physiol. A Mol. Integr. Physiol* 155 (2010) 123–133. [PubMed: 19770066]
- [16]. Soulages JL, Arrese EL, Dynamics and hydration of the alpha-helices of apolipoprotein III, *J. Biol. Chem* 275 (2000) 17501–17509. [PubMed: 10748149]
- [17]. Dwivedi P, Rodriguez J, Ibe NU, Weers PM, Deletion of the N- or C-terminal helix of apolipoprotein III to create a four-helix bundle protein, *Biochemistry* 55 (2016) 3607–3615. [PubMed: 27280697]
- [18]. Dettloff M, Weers PM, Niere M, Kay CM, Ryan RO, Wiesner A, An N-terminal three-helix fragment of the exchangeable insect apolipoprotein apolipoprotein III conserves the lipid binding properties of wild-type protein, *Biochemistry* 40 (2001) 3150–3157. [PubMed: 11258930]

- [19]. Dettloff M, Niere M, Ryan RO, Luty R, Kay CM, Wiesner A, Weers PM, Differential lipid binding of truncation mutants of *Galleria mellonella* apolipoprotein III, *Biochemistry* 41 (2002) 9688–9695. [PubMed: 12135391]
- [20]. Narayanaswami V, Weers PM, Bogerd J, Kooiman FP, Kay CM, Scraba DG, Van der Horst DJ, Ryan RO, Spectroscopic and lipid binding studies on the amino and carboxyl terminal fragments of *Locusta migratoria* apolipoprotein III, *Biochemistry* 34 (1995) 11822–11830. [PubMed: 7547916]
- [21]. Hård K, Van Doorn JM, Thomas-Oates JE, Kamerling JP, Van der Horst DJ, Structure of the asn-linked oligosaccharides of apolipoprotein III from the insect *Locusta migratoria*. Carbohydrate-linked 2-aminoethylphosphonate as a constituent of a glycoprotein, *Biochemistry* 32 (1993) 766–775. [PubMed: 8422381]
- [22]. Whitmore L, Wallace BA, DICHROWEB, an online server for protein secondary structure analyses from circular dichroism spectroscopic data, *Nucleic Acids Res* 32 (2004) W668–W673. [PubMed: 15215473]
- [23]. Pettersen EF, Goddard TD, Huang CC, Couch GS, Greenblatt DM, Meng EC, Ferrin TE, UCSF Chimera—a visualization system for exploratory research and analysis, *J. Comput. Chem* 25 (2004) 1605–1612. [PubMed: 15264254]
- [24]. Van der Horst DJ, Van Doorn JM, Voshol H, Kanost MR, Ziegler R, Beenackers AM, Different isoforms of an apoprotein (apolipoprotein III) associate with lipoproteins in *Locusta migratoria*, *Eur. J. Biochem* 196 (1991) 509–517. [PubMed: 2007409]
- [25]. Roccatano D, Colombo G, Fioroni M, Mark AE, Mechanism by which 2,2,2-trifluoroethanol/water mixtures stabilize secondary-structure formation in peptides: a molecular dynamics study, *Proc. Natl. Acad. Sci. U. S. A* 99 (2002) 12179–12184. [PubMed: 12196631]
- [26]. Weers PM, Prenner EJ, Kay C, Ryan RO, Lipid binding of the exchangeable apolipoprotein apolipoprotein III induces major changes in fluorescence properties of tryptophans 115 and 130, *Biochemistry* 39 (2000) 6874–6880. [PubMed: 10841768]
- [27]. Liu H, Scraba DG, Ryan RO, Prevention of phospholipase-C induced aggregation of low density lipoprotein by amphipathic apolipoproteins, *FEBS Lett* 316 (1993) 27–33. [PubMed: 8422936]
- [28]. Segrest JP, Garber DW, Brouillette CG, Harvey SC, Anantharamaiah GM, The amphipathic alpha helix: a multifunctional structural motif in plasma apolipoproteins, *Adv. Protein Chem* 45 (1994) 303–369. [PubMed: 8154372]
- [29]. Weers PM, Kay CM, Ryan RO, Conformational changes of an exchangeable apolipoprotein, apolipoprotein III from *Locusta migratoria*, at low pH: correlation with lipid binding, *Biochemistry* 40 (2001) 7754–7760. [PubMed: 11412130]
- [30]. Soulages JL, Bendavid OJ, The lipid binding activity of the exchangeable apolipoprotein apolipoprotein-III correlates with the formation of a partially folded conformation, *Biochemistry* 37 (1998) 10203–10210. [PubMed: 9665727]
- [31]. Weers PM, Narayanaswami V, Ryan RO, Modulation of the lipid binding properties of the N-terminal domain of human apolipoprotein E3, *Eur. J. Biochem* 268 (2001) 3728–3735. [PubMed: 11432739]
- [32]. Morrow JA, Hatters DM, Lu B, Hochtl P, Oberg KA, Rupp B, Weisgraber KH, Apolipoprotein E4 forms a molten globule A potential basis for its association with disease, *J. Biol. Chem* 277 (2002) 50380–50385. [PubMed: 12393895]
- [33]. Mei X, Atkinson D, Lipid-free apolipoprotein A-I structure: insights into HDL formation and atherosclerosis development, *Arch. Med. Res* 46 (2015) 351–360. [PubMed: 26048453]
- [34]. Beckstead JA, Block BL, Bielicki JK, Kay CM, Oda MN, Ryan RO, Combined N- and C-terminal truncation of human apolipoprotein A-I yields a folded, functional central domain, *Biochemistry* 44 (2005) 4591–4599. [PubMed: 15766290]
- [35]. Melchior JT, Walker RG, Cooke AL, Morris J, Castleberry M, Thompson TB, Jones MK, Song HD, Rye K-A, Oda MN, Sorci-Thomas MG, Thomas MJ, Heinecke JW, Mei X, Atkinson D, Segrest JP, Lund-Katz S, Phillips MC, Davidson WS, A consensus model of human apolipoprotein A-I in its monomeric and lipid-free state, *Nat. Struct. Mol. Biol* 24 (2017) 1093–1099. [PubMed: 29131142]

- [36]. Sevugan Chetty P, Mayne L, Kan ZY, Lund-Katz S, Englander SW, Phillips MC, Apolipoprotein A-I helical structure and stability in discoidal high-density lipoprotein (HDL) particles by hydrogen exchange and mass spectrometry, *Proc. Natl. Acad. Sci. U. S. A* 109 (2012) 11687–11692. [PubMed: 22745166]
- [37]. Nagao K, Hata M, Tanaka K, Takechi Y, Nguyen D, Dhanasekaran P, Lund-Katz S, Phillips MC, Saito H, The roles of C-terminal helices of human apolipoprotein A-I in formation of high-density lipoprotein particles, *Biochim. Biophys. Acta* 1841 (2014) 80–87. [PubMed: 24120703]
- [38]. Narayanaswami V, Wang J, Schieve D, Kay CM, Ryan RO, A molecular trigger of lipid binding-induced opening of a helix bundle exchangeable apolipoprotein, *Proc. Natl. Acad. Sci. U. S. A* 96 (1999) 4366–4371. [PubMed: 10200268]
- [39]. Weers PM, Narayanaswami V, Kay CM, Ryan RO, Interaction of an exchangeable apolipoprotein with phospholipid vesicles and lipoprotein particles. Role of leucines 32, 34, and 95 in *Locusta migratoria* apolipoprotein III, *J. Biol. Chem* 274 (1999) 21804–21810. [PubMed: 10419496]
- [40]. Weise C, Franke P, Kopáček P, Wiesner A, Primary structure of apolipoprotein-III from the greater wax moth, *Galleria mellonella*, *J. Protein Chem* 17 (1998) 633–641. [PubMed: 9853677]
- [41]. Zdybicka-Barabas A, St czek S, Mak P, Skrzypiec K, Mendyk E, Cytry ska M, Synergistic action of *Galleria mellonella* apolipoprotein III and lysozyme against Gram-negative bacteria, *Biochim. Biophys. Acta* 1828 (2013) 1449–1456. [PubMed: 23419829]
- [42]. Narayanaswami V, Kay CM, Oikawa K, Ryan RO, Structural and binding characteristics of the carboxyl terminal fragment of apolipoprotein III from *Manduca sexta*, *Biochemistry* 33 (1994) 13312–13320. [PubMed: 7947739]
- [43]. Rathnayake SS, Mirheydari M, Schulte A, Gillahan JE, Gentit T, Phillips AN, Okonkwo RK, Burger KNJ, Mann EK, Vaknin D, Bu W, Agra-Kooijman DM, Kooijman EE, Insertion of apoLp-III into a lipid monolayer is more favorable for saturated, more ordered, acyl-chains, *Biochim. Biophys. Acta* 1838 (2014) 482–492. [PubMed: 24099741]
- [44]. Mirheydari M, Mann EK, Kooijman EE, Interaction of a model apolipoprotein, apoLp-III, with an oil-phospholipid interface, *Biochim. Biophys. Acta Biomembr* 1860 (2018) 396–406. [PubMed: 29030246]
- [45]. Garda HA, Arrese EL, Soulages JL, Structure of apolipoprotein-III in discoidal lipoproteins Interhelical distances in the lipid-bound state and conformational change upon binding to lipid, *J. Biol. Chem* 277 (2002) 19773–19782. [PubMed: 11896049]
- [46]. Sahoo D, Weers PMM, Ryan RO, Narayanaswami V, Lipid-triggered conformational switch of apolipoprotein III helix bundle to an extended helix organization, *J. Mol. Biol* 321 (2002) 201–214. [PubMed: 12144779]
- [47]. Bibow S, Polyhach Y, Eichmann C, Chi CN, Kowal J, Albiez S, McLeod RA, Stahlberg H, Jeschke G, Güntert P, Riek R, Solution structure of discoidal high-density lipoprotein particles with a shortened apolipoprotein A-I, *Nat. Struct. Mol. Biol* 24 (2017) 187–193. [PubMed: 28024148]

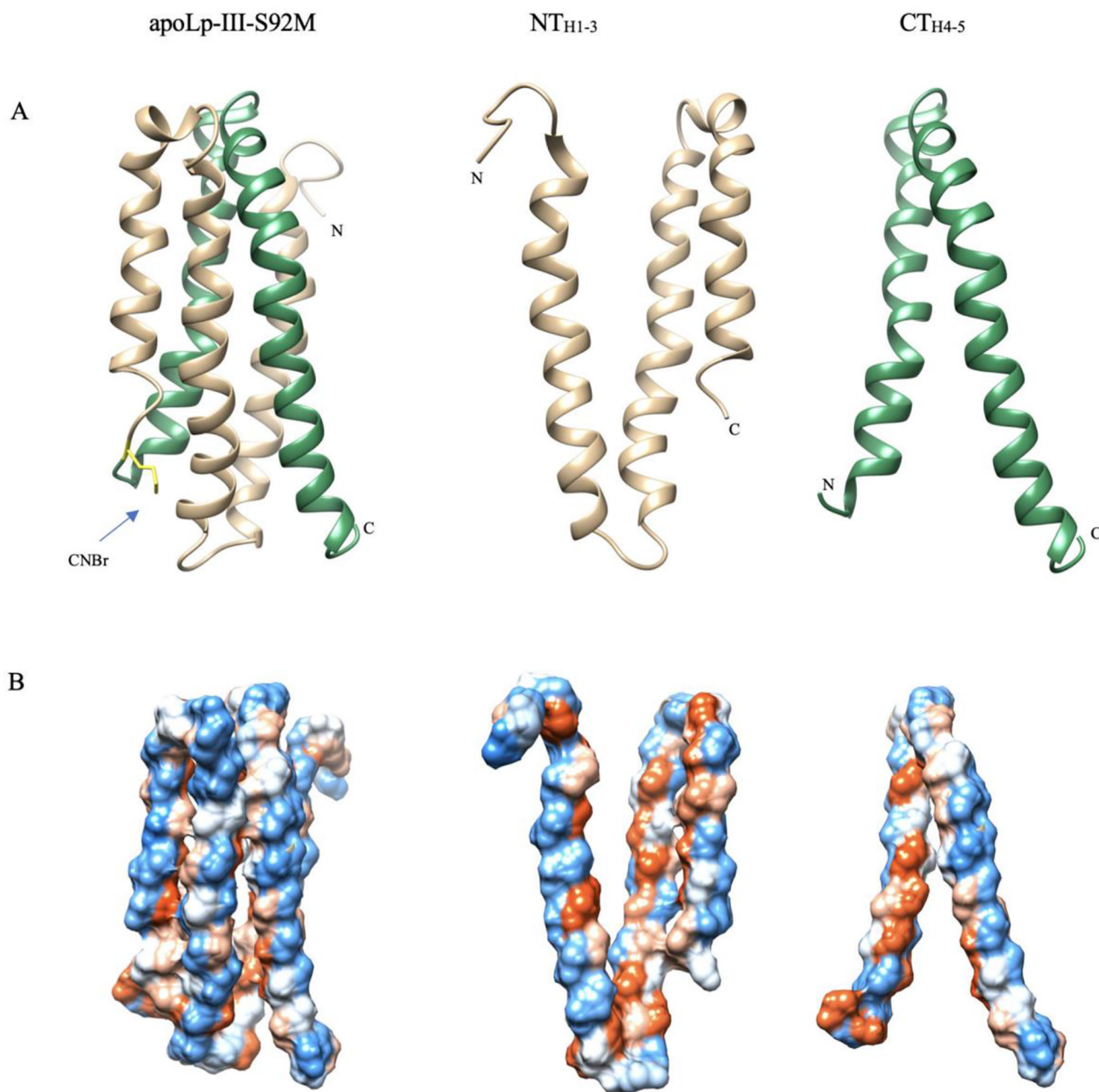


Fig. 1. ApoLp-III-S92M and fragments generated by CNBr cleavage. The NMR solution structure of apoLp-III_{LM} is shown in panel A on the left with the three NT helices (grey) and the two CT helices (green). The position of the S92M mutation is shown in yellow, and CNBr digestion produced the NT_{H1-3} (rotated 180°) and CT_{H4-5} fragments. Surface contour in Panel B indicates the degree of hydrophobicity with a color gradient of blue (hydrophilic) to red (hydrophobic), showing the increased exposed hydrophobic surface of two fragments (For interpretation of the references to color in this figure legend, the reader is referred to the web version of this article.).

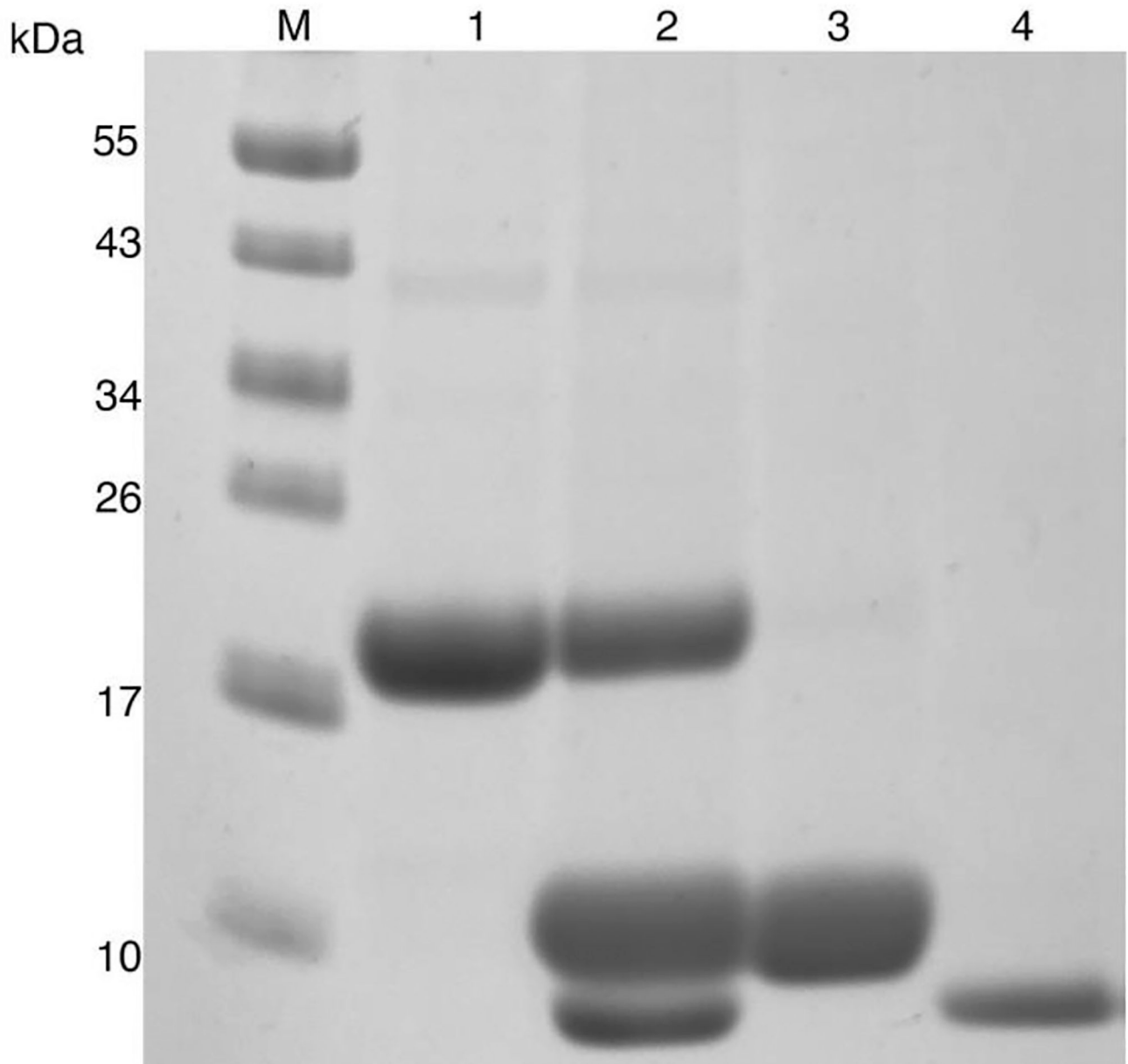


Fig. 2. SDS-PAGE of CNBr digest of apoLp-III-S92M Lane M: Marker protein with molecular masses indicated on the left; lane 1: apoLp-III-S92M; lane 2: CNBr digest of apoLp-III-S92M; lane 3 and 4 show the two fragments purified by reversed-phase HPLC: NT_{H1-3} (lane 3) and CT_{H4-5} (lane 4).

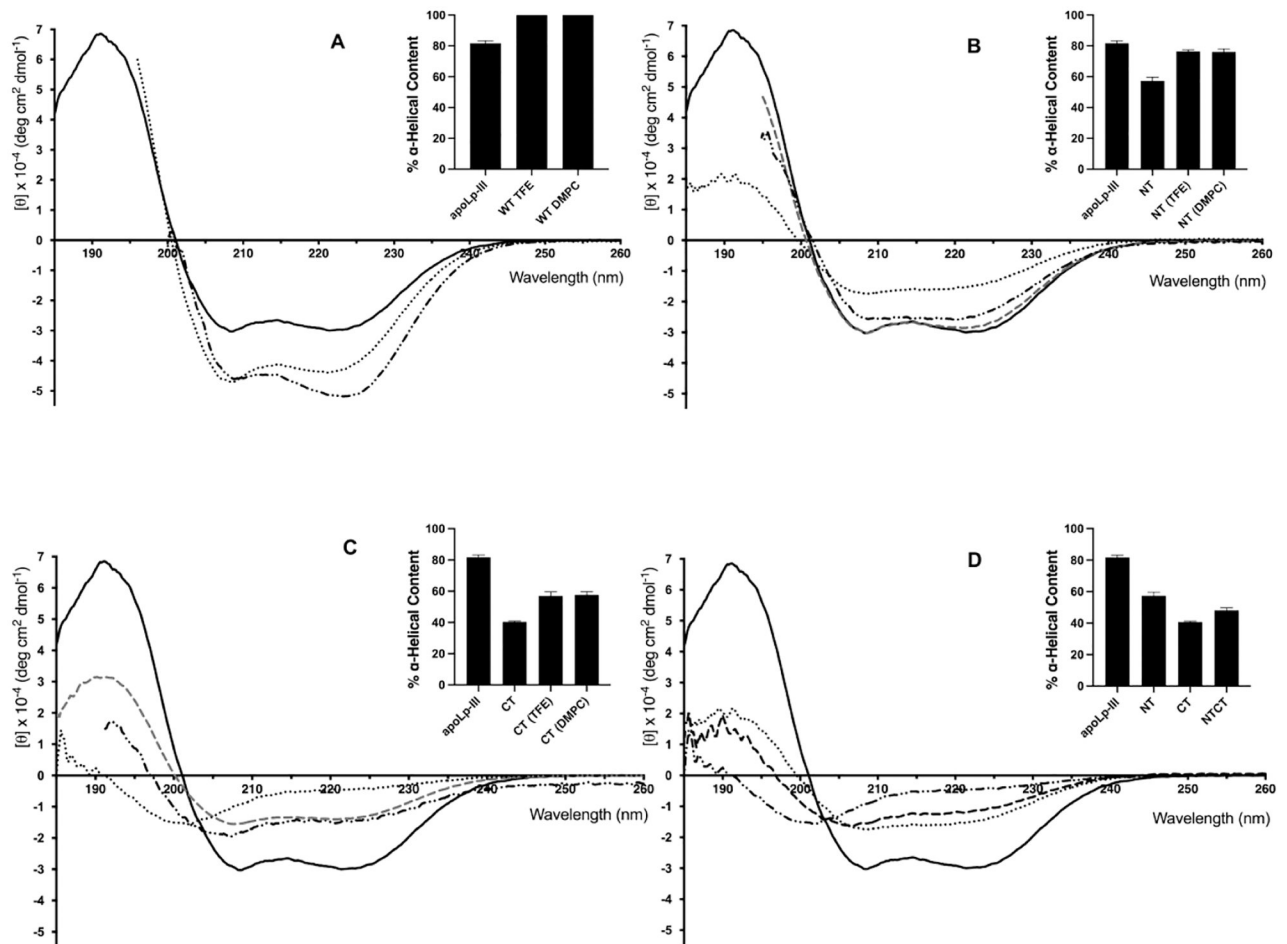


Fig. 3.

Far UV CD analysis of the apoLp-III fragments. Shown are CD scans of apoLp-III and the two fragments in buffer, at a protein concentration of 0.2 mg/mL. The CD scans are the average of three separate measurements while the corresponding bar graph shows the % α -helical content of each protein using CDSSTR (\pm SD, $n = 3$). Panel A shows intact apoLp-III (solid line), and in the presence of 50% TFE (dotted) or DMPC (dash-dotted). Panel B shows intact apoLp-III (solid line), and apoLp-III-NT_{H1-3} in the absence (dotted) or presence of 50% TFE (dashed) or DMPC (dash-dotted). Panel C shows intact apoLp-III (solid line), and apoLp-III-CT_{H4-5} in the presence of 50% TFE (dashed) or DMPC (dash-dotted). Panel D shows intact apoLp-III (solid line), NT_{H1-3} (dotted), CT_{H4-5} (dash-dotted), and the mixture of NT_{H1-3} and CT_{H4-5} (dashed).

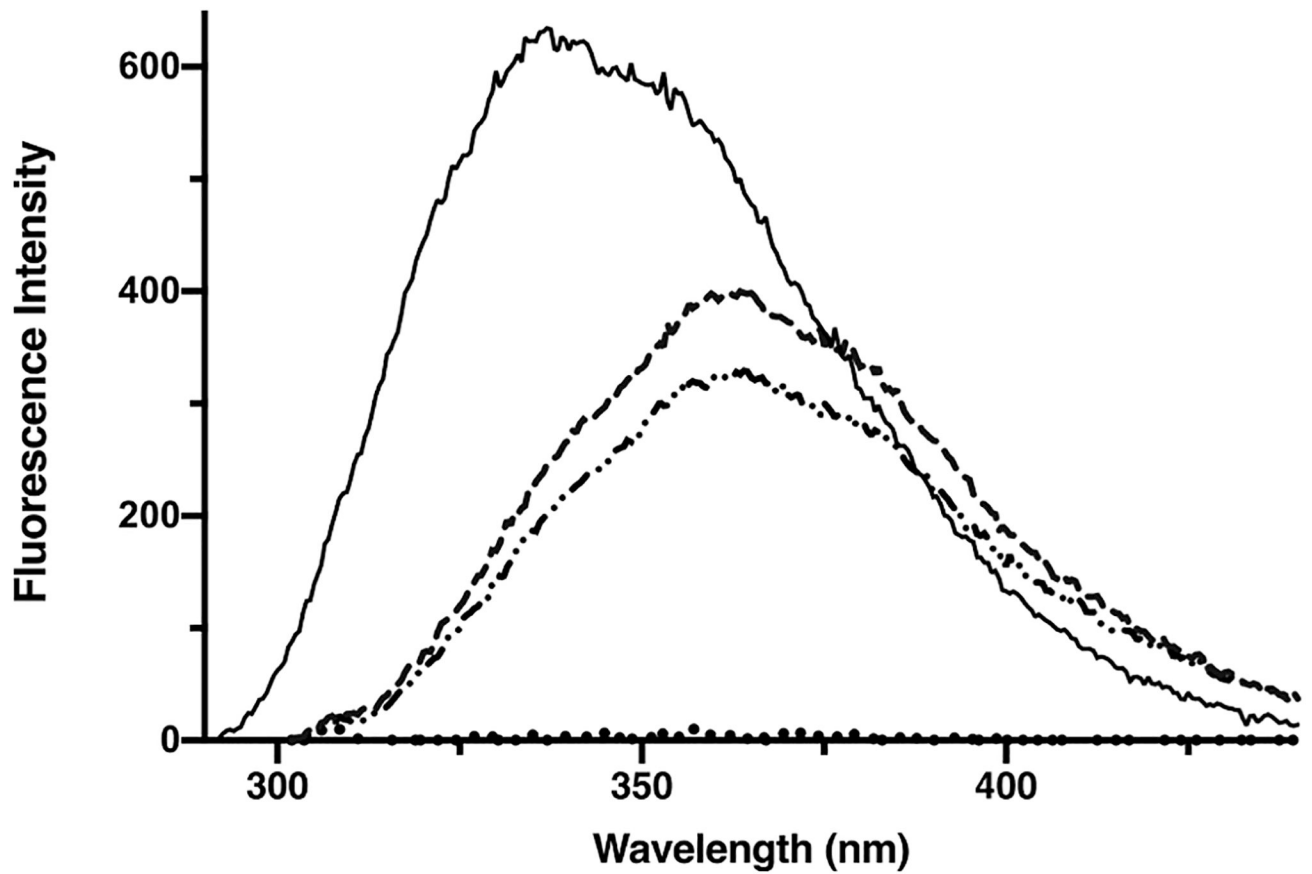


Fig. 4. Tryptophan Fluorescence. ApoLp-III samples (30 $\mu\text{g}/\text{mL}$) were excited at 280 nm and the emission intensity was measured between 290 and 460 nm. Shown are NT_{H1-3} (dotted line), CT_{H4-5} (dashed line), the NT_{H1-3}/CT_{H4-5} mixture (dash-dotted line), and intact apoLp-III (solid line). The emission profiles are the average of three independent scans for each protein.

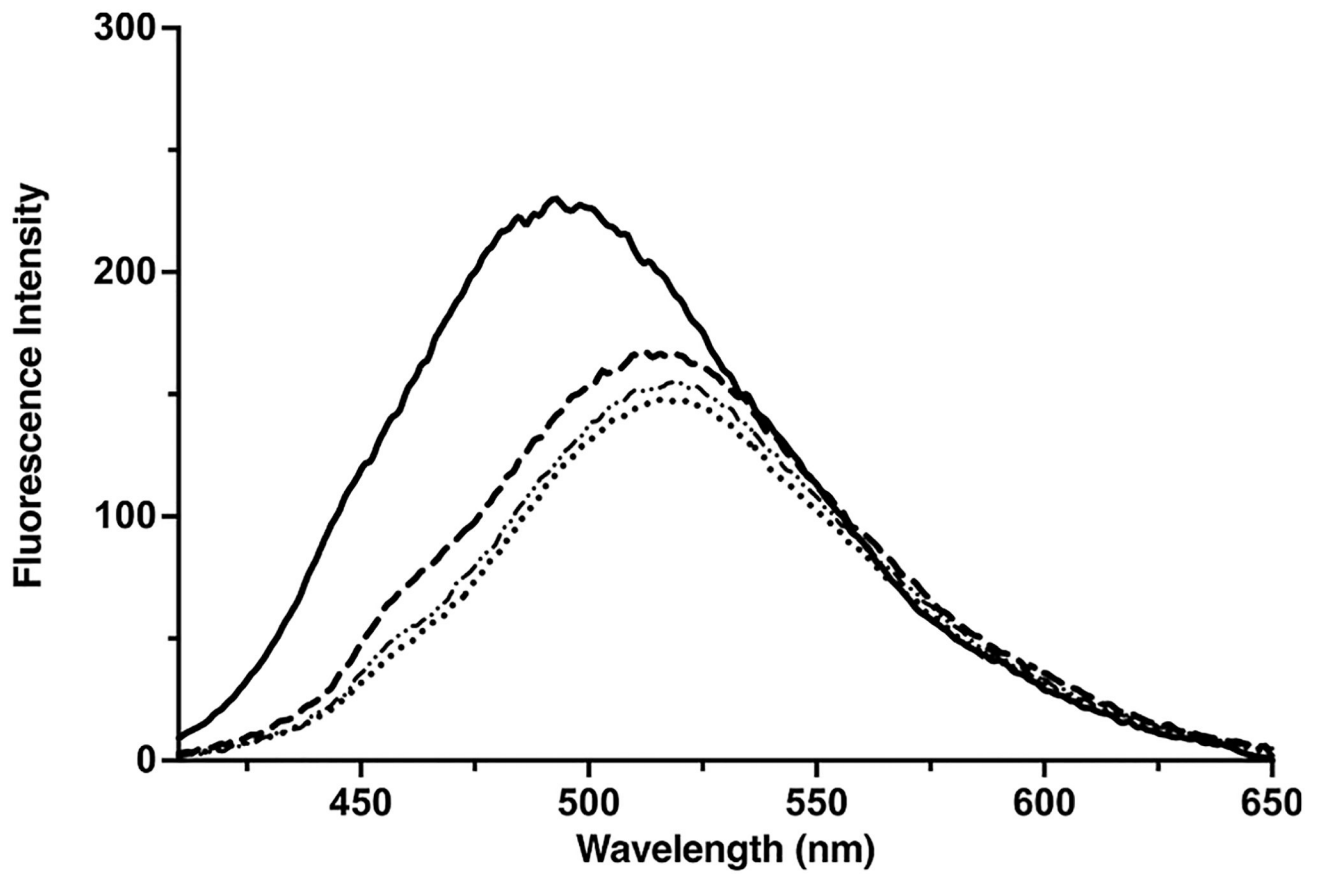


Fig. 5. ANS Fluorescence. Protein samples (5 μ M) were excited at 395 nm and the emission intensity was measured between 400 and 650 nm. Shown are intact apoLp-III (solid line), NT_{H1-3} (dashed line), CT_{H4-5} (dash-dotted line), and ANS in the absence of protein (dotted line). The emission profiles are the average of three independent scans for each protein.

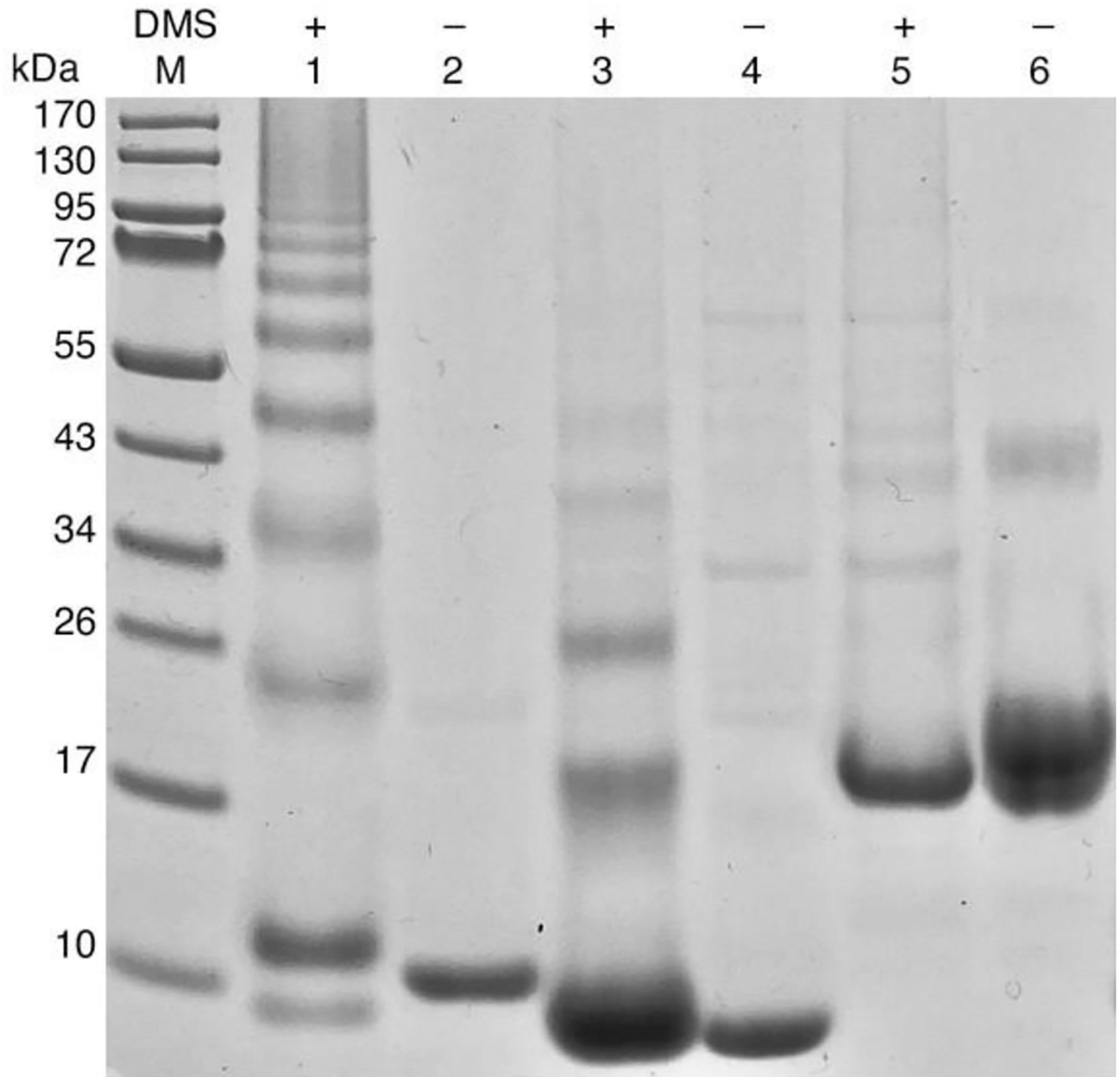


Fig. 6. SDS-PAGE of DMS protein crosslinking. Protein samples (0.75 mg/mL) were incubated with DMS and crosslinked proteins were analyzed by SDS-PAGE. Shown are apoLp-III-NT_{H1-3} in the presence (lane 1) or absence of DMS (lane 2), apoLp-III-CT_{H4-5} in the presence (lane 3) or absence of DMS (lane 4), intact apoLp-III in the presence (lane 5) or absence of DMS (lane 6). Lane M contains marker proteins with molecular masses indicated on the left.

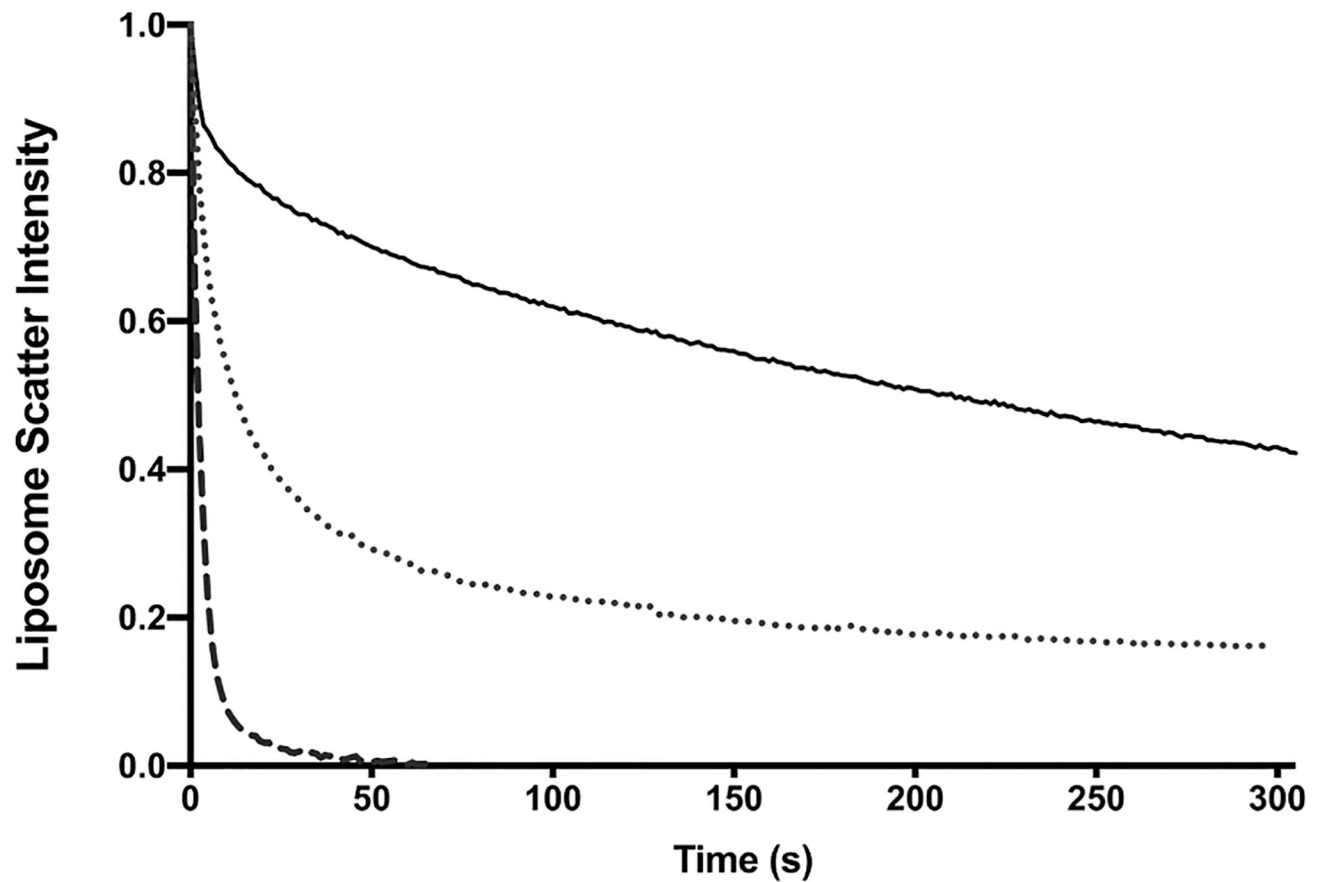


Fig. 7. DMPC vesicle solubilization. LUVs made of DMPC were incubated in the presence of protein (0.125 mg/mL) at a 2:1 weight ratio of lipid to protein at 24.1 °C. Vesicle solubilization was monitored by light scatter intensity at 325 nm. Shown are intact apoLp-III (solid line), NT_{H1-3} (dotted), and CT_{H4-5} (dashed) fragments.

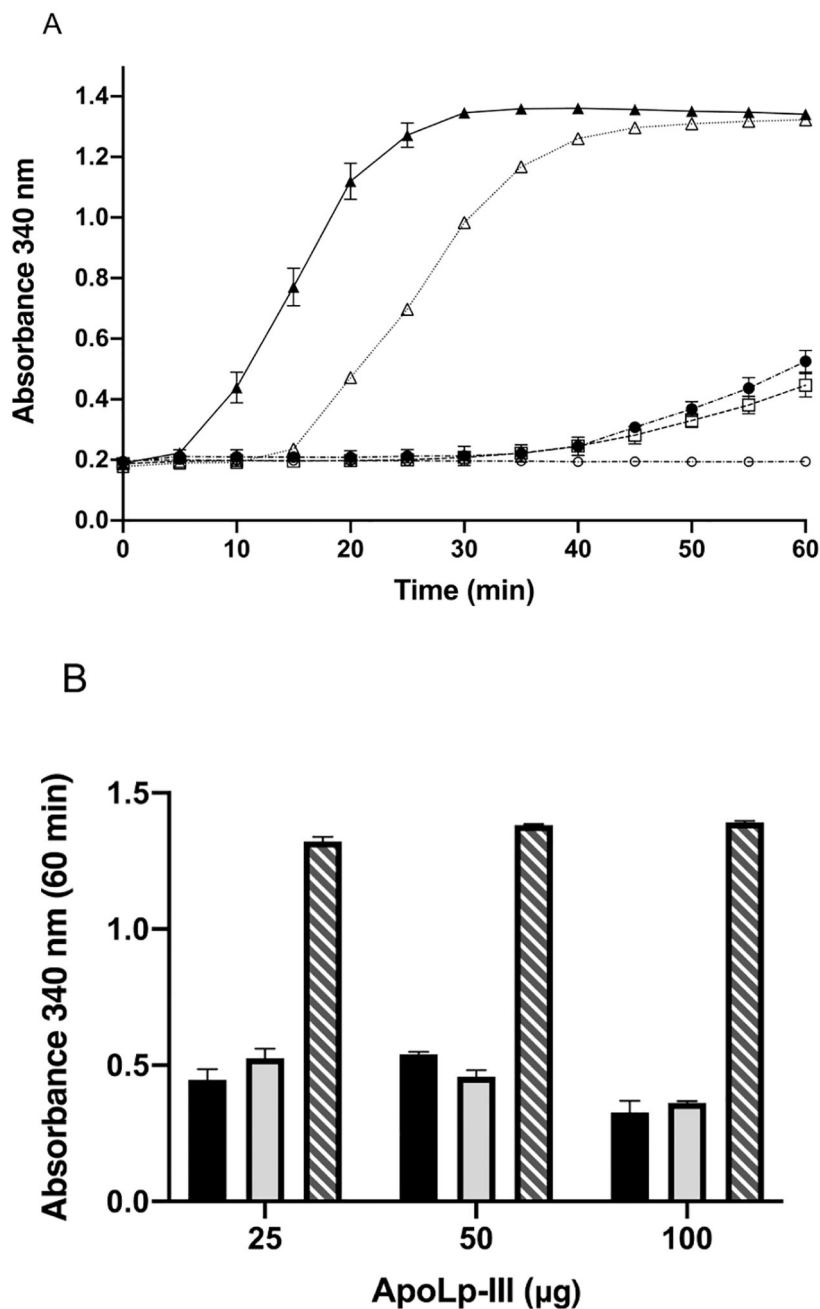


Fig. 8. PL-C induced LDL aggregation. Panel A: LDL and 160 mU of PL-C were mixed incubated at 37 °C, and the absorbance at 340 nm measured at 5 min intervals. Shown are LDL (open circles), LDL with PLC in the absence of protein (closed triangles), and in the presence of 25 µg (0.125 mg/mL) of intact apoLp-III (open squares), NT_{H1-3} (closed circles), and CT_{H4-5} fragments (open triangles). Panel B shows the absorbance at the 60 min timepoint in the presence of 25, 50, and 100 µg intact apoLp-III (black), NT_{H1-3} (grey), or CT_{H4-5} (diagonal hatched pattern).

Table 1

Summary of Helical content.

	Θ_{222}	CDSSTR	Contin	Selcon3
apoLp-III				
Buffer	82.0 ± 1.9	81.7 ± 1.5	77.3 ± 0.6	75.0 ± 1.7
TFE	100.0	89.3 ± 0.7	100.0	100.0
DMPC	100.0	84.3 ± 0.3	100.0	100.0
NT_{H1-3}				
Buffer	48.7 ± 3.5	57.3 ± 2.3	58.0 ± 0.3	57.7 ± 4.0
TFE	72.6 ± 1.4	76.3 ± 1.2	63.1 ± 3.2	62.9 ± 2.5
DMPC	71.5 ± 3.2	76.0 ± 2.0	71.5 ± 0.7	65.0 ± 1.9
CT_{H4-5}				
Buffer	19.6 ± 0.5	41.0 ± 0.6	43.7 ± 2.3	43.5 ± 0.6
TFE	42.5 ± 0.4	57.0 ± 2.6	58.5 ± 0.8	62.5 ± 1.7
DMPC	44.8 ± 1.5	57.7 ± 2.1	56.0 ± 4.9	50.3 ± 2.4
NT_{H1-3} & CT_{H4-5}				
Buffer	48.0 ± 1.7	48.0 ± 1.7	52.2 ± 1.4	52.5 ± 3.0
TFE	91.0 ± 3.6	91.0 ± 3.6	63.8 ± 0.0	76.1 ± 1.0

% α -Helical content was calculated from three separate trials utilizing the DICHROWEB CDSSTR "Soluble Protein" 175 algorithm and $[\Theta]_{222}$ (average ± SD).